HPD COURIER

FAIR
CONSTRUCTION SITE

CBM cave before ceiling

CMB Phase 0 - mCBM testing setup

CONTENTS

ACHIEVEMENTS

EVENTS

ACHIEVEMENTS

Nuclear Structure and Dynamics

Isospin-symmetry breaking in the A = 62 isovector triplet

Due to exotic tiny effects induced by the isospin-symmetry breaking, nuclei at or near the N = Z line continue to be in the foreground of nuclear structure research. Apart from displaying some rather interesting nuclear structure effects, the superallowed $0^+ \rightarrow 0^+$ Fermi β-decay of these nuclei is a valuable tool providing tests of the validity of the conserved-vector-current (CVC) hypothesis and the unitarity of the Cabibbo-Kobayashi-Maskawa (CKM) matrix.
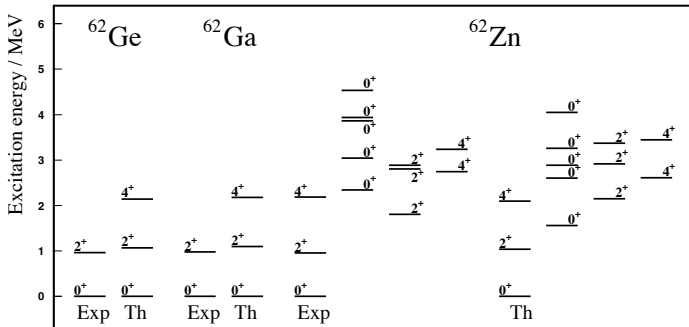
We have studied the effects of isospin mixing on Coulomb energy differences, mirror energy differences, triplet energy differences, and superallowed Fermi β^+-decay in the A = 62 (Ge-Ga-Zn) isovector triplet investigating the yrast states up to spin 4^+ of these nuclei and the Fermi β-decay of the ground states of $^{62}$Ge and ^{62}Ga in the framework of the *complex* Excited VAMPIR (EXVAM) model using an effective interaction obtained from a G-matrix renormalised for the A $\approx$ 70 mass region starting from the charge-dependent Bonn CD potential.

The main prolate deformed configuration in the structure of the ground state represented ~94% of the total amplitude of the wave function while the amount of mixing for the yrast 2^+ and 4^+ states varied from 10% to 14% in the isovector triplet ^{62}Ge-^{62}Ga-^{62}Zn. The analysed electromagnetic properties of the yrast states in ^{62}Zn, B(E2) transition strengths and g-factors, were found to be in agreement with the experimental data.

The influence of shape coexistence and mixing in the structure of the involved states on the superallowed Fermi β^+-decay is also investigated. We have found that the depletion of the ground-to-ground transition amounts to 0.74% for the ^{62}Ge and 0.75% for the ^{62}Ga ground-state decay, the missing strength being distributed over many 0^+ excited states.
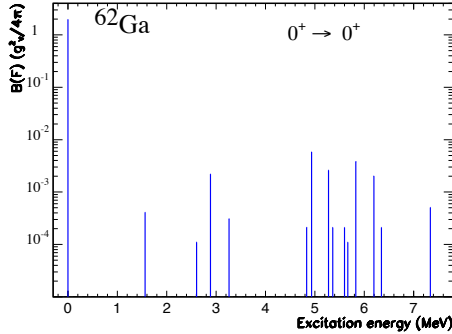
The results, presented in the figure for ^{62}Ga decay, include both the isospin-symmetry-breaking interactions and shape coexistence and mixing effects. EX-VAM calculations reveal weak decay branches feeding the lowest few excited 0^+ states in agreement with recent experimental data.

The present results represent the first beyond-mean-field investigation of the A = 62 isovector triplet self-consistently treating the interplay between the isospin-symmetry-breaking and shape coexistence and mixing effects.

For details

A. Petrovici, O.Andrei, A. S. Mare, AIP Conference Proceedings 2076, 020001 (2019)
A. Petrovici, Phys. Rev. C 91, 014302 (2015)
A. Petrovici, K. W. Schmid, O. Radu, A. Faessler, Phys. Rev. C 78, 064311 (2008)

Strongly Interacting Matter

Charged particles and π^0 suppresion in heavy ion collisions

As it is known by now, one of the powerful tools used to diagnose the properties of deconfined matter produced in relativistic heavy-ion collisions is the study of the energy loss of partons in such medium. The energy loss of a parton traversing deconfined matter, via collisional or radiative processes, will modify the transverse momentum (p_T) distributions of different particle species produced at the hadronization phase relative to the one corresponding to the minimum bias (MB) nucleon-nucleon collision at the same energy, where such deconfined matter is not produced. Based on these considerations and on experimentally measured observables, the nuclear modification factor (R_{AA}) as the ratio of the p_T spectra at a given centrality in heavy ion collisions to the spectrum of proton-proton (pp) MB collisions at the same collision energy, multiplied by the number of binary collisions ($\langle N_{bin} \rangle$), can be estimated.
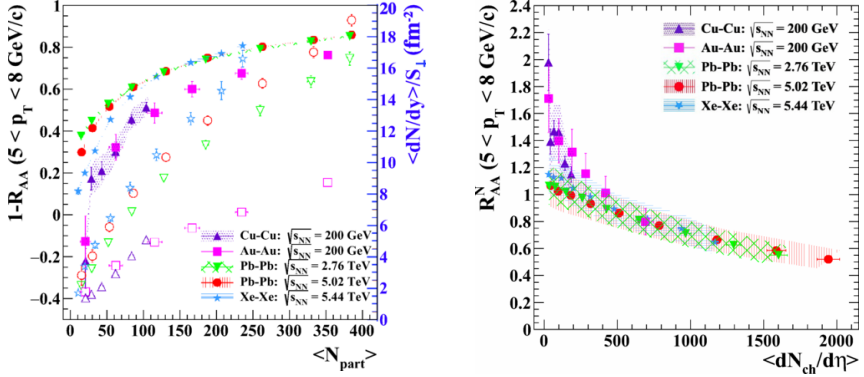
In the cases where experimental data are not available for pp collisions at the same collision energy, one can estimate the nuclear modification factor (R_{CP}) defined as the ratio of the p_T spectra at a given centrality to the spectrum in peripheral collisions, each of them divided to the corresponding number of binary collisions. Recently, based on the experimental results obtained at the Relativistic Heavy Ion Collider (RHIC) for Au-Au and Cu-Cu and at the Large Hadron Collider (LHC) for Pb-Pb and Xe-Xe collisions, a detailed analysis of the charged particle suppression in the region of transverse momentum corresponding to the maximum suppression ($5 < p_T < 8$ GeV/c) was done.

As can be seen in the top left figure, for an average number of participating nucleons $\langle N_{part} \rangle$ corresponding to central Xe-Xe collisions, the differences in $\langle dN/dy \rangle / S_\perp$ (open symbols-right scale) for Pb-Pb at $\sqrt{s_{NN}}=2.76$, 5.02 TeV and for Xe-Xe at $\sqrt{s_{NN}}=5.44$ TeV, relative to Au-Au at $\sqrt{s_{NN}}=200$ GeV are increasing with the collision energy, while the differences in ($1-R_{AA}$) (full symbols - left scale) are the same within the error bars. For central Au-Au collisions, where the difference in $\langle dN/dy \rangle / S_\perp$ between Pb-Pb at $\sqrt{s_{NN}}=2.76$ TeV and Au-Au at $\sqrt{s_{NN}}=200$ GeV is relatively large, the difference in ($1-R_{AA}$) is almost negligible. This suggests a suppression saturation at LHC energies.

R_{AA}, as a measure of the suppression in heavy ion collisions, is based on the estimates of $\langle N_{bin} \rangle$ within the Glauber Monte Carlo approach, where straight trajectories are used as hypothesis. The dependence on the collision energy is introduced by the nucleon-nucleon cross section along with the oversimplified assumption that every nucleon-nucleon collision takes place at the same collision energy ($\sqrt{s}$) and, consequently, the same cross section (σ_{pp}).

R_{AA}^N is estimated as a ratio of the p_T spectra in A-A collisions to the one in MB pp collisions at the same collision energy, each of them normalised to the corresponding mean charged particle densities ($\langle dN_{ch}/d\eta \rangle$):

$$R_{AA}^N = \frac{(\frac{d^2N}{dp_T d\eta} / \langle \frac{dN_{ch}}{d\eta} \rangle)^{cen}}{(\frac{d^2N}{dp_T d\eta} / \langle \frac{dN_{ch}}{d\eta} \rangle)^{pp,MB}}$$

Thus, R_{AA}^N is based only on experimentally measured observables and it can also be used in the case of pp collisions, where the numerator is calculated for a given multiplicity range. The R_{AA}^N as a function of $\langle dN_{ch}/d\eta \rangle$ for the same systems is presented in the top right figure.

The geometrical scaling shows that for the highest charged particle multiplicity in pp collisions at $\sqrt{s}$=7 TeV, the average transverse flow velocity ($\langle \beta_T \rangle$) in pp and in Pb-Pb collisions at $\sqrt{s_{NN}}$=2.76 TeV is the same. Therefore, the contribution of the hydrodynamic expansion to the suppression plays a similar role.

Assuming the same jet-medium coupling, $(1\text{-}R_{pp}^{N(HM)})/\ (1\text{-}R_{AA}^N(\langle N_{part} \rangle = 125)) \approx S_\perp^{pp,HM} /\ S_\perp^{Pb-Pb,\langle N_{part} \rangle=125}$.

This could explain why in pp collisions at LHC, in high charged particle multiplicity (HM) events, in the limit of current experimental uncertainties, no suppression was observed, although similarities to Pb-Pb collisions for other observables were evidenced.

The ratios $(1 - R_{AA}^{\pi^0})/\langle dN/dy \rangle$ (a) and $[1 - (R_{AA}^N)^{\pi^0}]/\langle dN/dy \rangle$ (b) (black markers - left scale) as a function of collision energy, show a maximum around the top RHIC energies (in the region of $\sqrt{s_{NN}} = 62.4$ - 130 GeV), decreasing towards LHC energies (in the figure on the right) in qualitative agreement with theoretical predictions.
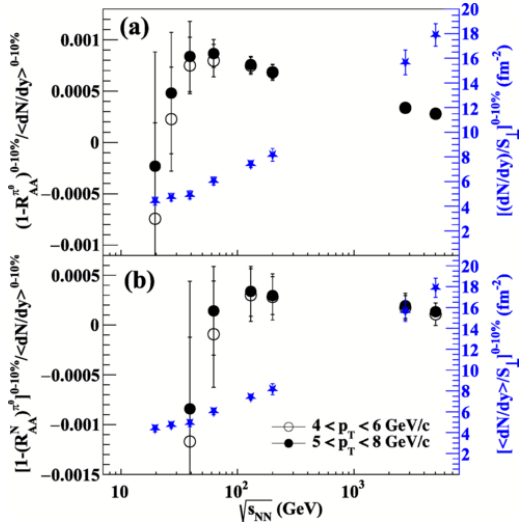
To what extent such a trend is due to a transition from a magnetic plasma of light monopoles near the critical temperature region to a deconfined matter dominated by quarks and gluons remains an open question. However, the trends in the experimental data suggest a change in the properties of the deconfined matter from RHIC to LHC energies.

For details

M. Petrovici, A. Lindner and A. Pop, Phys. Rev. C 103 (2021) 034903

M. Petrovici, Talk: 40th International Conference on High Energy Physics 2020

M. Petrovici, A. Lindner and A. Pop, AIP Conf. Proc. 2076 (2019) 040001

Geometrical scaling for strange and multi-strange hadrons

The experimental results obtained in hadron collisions at the Large Hadron Collider (LHC) energies, at high charged particle densities, are a strong testing ground for Quantum Chromodynamics (QCD) in the weak coupling approximation. The success of the Color Glass Condensate (CGC) theoretical model for the pre-partonic phase in such collisions shows that small x degrees of freedom which dominate the particle production at LHC energies, can be described. Based on this approach and on the local parton-hadron duality, predictions on the behaviour of the $\langle p_T \rangle / \sqrt{(dN/dy)/S_\perp}$ ratio as a function of collision energy and centrality have been made. The expected behaviour of $\langle p_T \rangle / \sqrt{(dN/dy)/S_\perp}$ as a function of collision energy and centrality for a wide range of energies and for different collision systems at the same collision energy was systematically investigated in one of our previous papers for π^+, K^+ and p. These studies were extended to single and multi-strange hadrons.
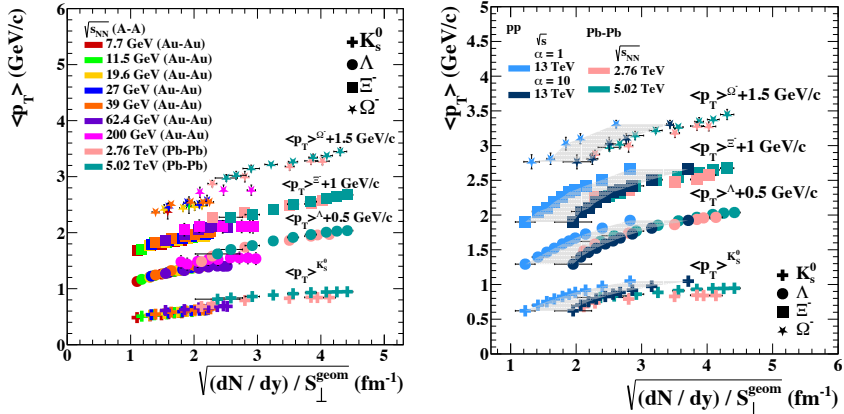

Results for the $\langle p_T \rangle$ dependence on $\sqrt{(dN/dy)/S_\perp}$ are presented (left figure) for strange and multi-strange hadrons (an offset in $\langle p_T \rangle$ was added for a better visualisation). A wide range of energies is studied, from $\sqrt{s_{NN}} = 7.7$ GeV up to 39 GeV measured in the Beam Energy Scan (BES) program and the intermediate and highest energies measured at the Relativistic Heavy Ion Collider (RHIC) ($\sqrt{s_{NN}} = 62.4$ and 200 GeV) in Au-Au collisions, up to $\sqrt{s_{NN}} = 2.76$ and 5.02 TeV measured at LHC for Pb-Pb collisions.

A very good scaling is observed from the lowest BES energy, up to the highest energy measured at RHIC, where a trend towards saturation is evidenced. With an offset between RHIC and LHC energies, a very good scaling is also evidenced at the LHC energies. A comparison between pp and Pb-Pb collisions at LHC energies is done in terms of the dependence of $\langle p_T \rangle$ on $\sqrt{(dN/dy)/S_\perp}$ (right figure) for strange and multi-strange hadrons (an offset in $\langle p_T \rangle$ was added for a better visualisation). In the case of pp collisions, $S_\perp$ is estimated as the overlapping area corresponding to different values of the energy density of the Yang-Mill fields,

$\varepsilon = \alpha \Lambda_{QCD}^4$. A very good scaling is evidenced between Pb-Pb and pp collisions for $\alpha=10$. The border lines correspond to the two extreme values of α, 1 and 10. Since α can take any value in this range, the values in-between are represented with a gray shaded area.

A comparison between pp and Pb-Pb collisions in terms of the mean transverse flow velocity ($\langle\beta_T\rangle$) obtained by a simultaneous fit of the p_T spectra of different hadrons using the Boltzmann-Gibbs Blast Wave expression, inspired from hydrodynamical models, is presented in the right figure (top: π^+-K^+-p; bottom: strange and multi-strange hadrons K_s^0-Λ-Ξ^--Ω^-).
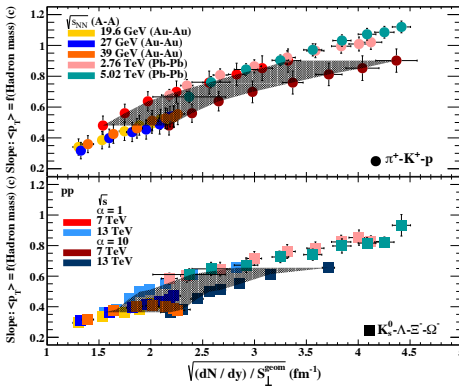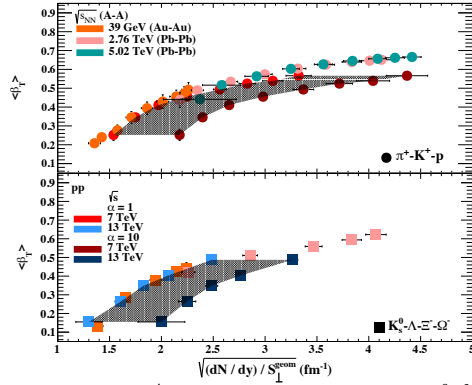
A representation in terms of the dependence of $\langle p_T \rangle$ on the hadron mass, based only on measured experimental data, is not biased by any model interpretation. Linear fits were performed separately for π^+, K^+ and p and K_s^0, Λ, Ξ^- and Ω^-, for different centralities (A-A) or multiplicity classes (pp). The results obtained for the slopes of the linear fits are presented in the figure on the left (top: π^+-K^+-p; bottom: strange and multi-strange

hadrons K_s^0-Λ-Ξ^--Ω^-).

One could conclude that, similar to π^+, K^+ and p, a good geometrical scaling is also evidenced for strange and multi-strange hadrons (K_s^0, Λ, Ξ^-, Ω^-) for A-A collisions. The dependence of the $\langle p_T \rangle$ on the CGC inspired geometrical variable shows an excellent scaling between Pb-Pb and pp collisions (for $\alpha=10$) at LHC energies. Observables that describe the dynamics of the collision, $\langle\beta_T\rangle$ and the slope of the $\langle p_T \rangle$-hadron mass dependence show a very good scaling between A-A and pp collisions, for $\alpha = 1$.

For details

A. Lindner, Talk: PANIC Conference 2021

A. Lindner, Poster: EPS-HEP Conference 2021

A. Lindner, M. Petrovici and A. Pop, arXiv:2111.07682; in print: PoS(PANIC2021)197

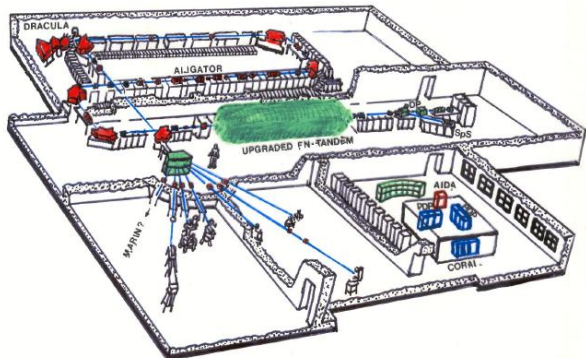M. Petrovici et al., Phys. Rev. C 98 (2018) 024904

The 30th anniversary of the first experiment with the DRACULA device at Laboratori Nazionali del Sud in Catania, Italy - a successful story

by Mihai Petrovici

The study of dissipative phenomena in heavy ion collisions was one of the main topics of nuclear physics once tandem, tandem + post-accelerators, linear accelerators or superconducting cyclotrons became operational. Following this trend, the project of a post-accelerator based on room temperature resonators using the existing FN Tandem, similar with the one in Max Plank Institute in Heidelberg, has been launched in the Heavy Ion Reactions (current Nuclear Physics) Department of our Institute, IFIN-HH.

Motivated by this, our group initiated in 1984 a rather ambitious project to build a versatile experimental set-up which was called DRACULA (**D**evice for **R**eaction **A**nalysis based on a **C**omplex and **U**nsurpassed on line **A**cquisition system) in order to make detailed studies of dissipative phenomena in the collision of light nuclei (Z≤20) at collision energies up to 40 MeV above the Coulomb barrier in the centre of mass for a symmetric system. Thus, the activities were concentrated on building new types of detectors: a twin large area position sensitive ionization chamber (IC), two large area parallel plate avalanche counters corresponding to the two halves of the IC, a position sensitive hybrid detector consisting of a single wire position sensitive proportional counter backed with a plastic scintillator strip, a combination of a Bragg geometry ionization chamber and a phoswich scintillator.

The DRACULA device was mounted just after the foreseen post- accelerator, as can be seen in the right figure. A dedicated effort to implement a complex and flexible **A**dvanced **I**PNE **D**ata **A**cquisition system (AIDA), based on commercially available multichannel ADC and TDC CAMAC mod-


ules interfaced to the PDP11/34 via a dedicated CAMAC Crate Controller 3912KS or to an Auxiliary Crate Controller J11, was initiated. Such an architecture was used in processing more than 50 parameters delivered by DRACULA experiment starting from 1986 during the commissioning phase and later, starting from 1991, in the experiments performed at Laboratori Nazionali del Sud (LNS) - Catania.
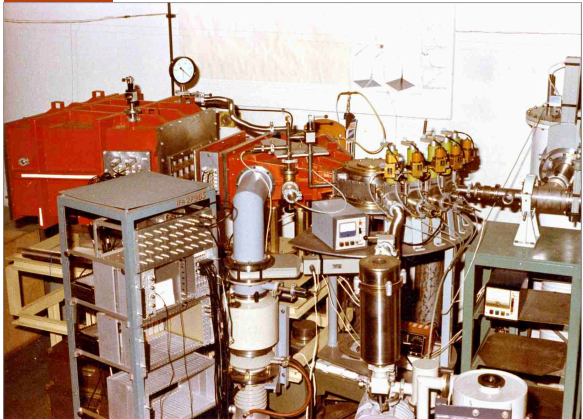
The main components of the DRACULA device were assembled (see left figure) and tested using different radioactive sources in 1986, the beam being not yet transported up to that area.

The results of some of such tests can be followed below.
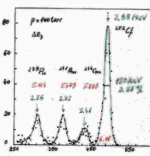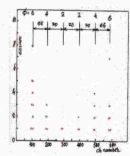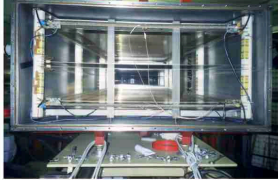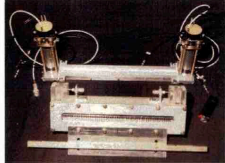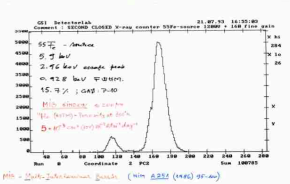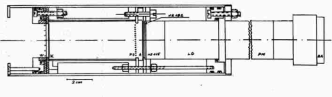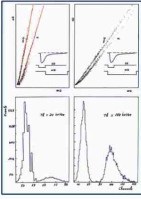
DAQ { AIDA
J11
PC
CAMDA

In the first half of 1986, a first test of the post-accelerator was performed for a couple of days. Some of the resonators were operated without re-bunching to access a good time resolution from the machine, the diagnosis was performed well upstream of our device, the transport elements up to our reaction chamber being not operational yet. In August 1986 a severe earthquake broke the column of

the Tandem accelerator with direct impact on the whole project. Tests of different components of the DRACULA device using radioactive sources continued, with the hope that the Tandem will be repaired and the post-accelerator will be operated at the expected parameters, which unfortunately did not happen.

In such circumstances, in May 1990, following the initiative of Giuseppe Guarino, a physicist from INFN Bari and an excellent collaborator in the period of his post-doctoral position at GSI-Darmstadt, invited me for a seminar at Bari for presenting the DRACULA device, its performance and physics topics that could be pursued using it. The seminar was followed by discussions during a couple of days within the group led by Ambrogio Pantaleo and the decision was to have a similar seminar and meeting with a group at L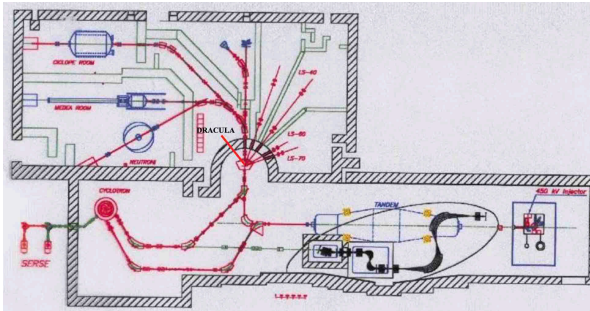NS and INFN Catania, Angelo Pagano, Gaetano Lanzanò and Giovanni Raciti. This decision was motivated by the existence at LNS of the 15 MV SMP Tandem accelerator and of the Superconducting Cyclotron, the construction of which was in the final stage.


The fruitful discussions were followed by a meeting with Emilio Migneco, the LNS Director who decided to make a special investment in equipping a dedicated transport line at 40 degrees for the DRACULA device (see left figure).

In Fall 1990 all components of the device were shipped to LNS and in May 1991 DRACULA was already assembled close to the final position in the target area at LNS.

In December 1991 DRACULA was placed in the final position, coupled to the beam line (see left figure), equipped with the front end electronics, vacuum systems, controlled gas flow in different sub-detectors, signal transport cables to the counting room, DAQ, etc. (see right figure) such that the first data were collected in the same month.
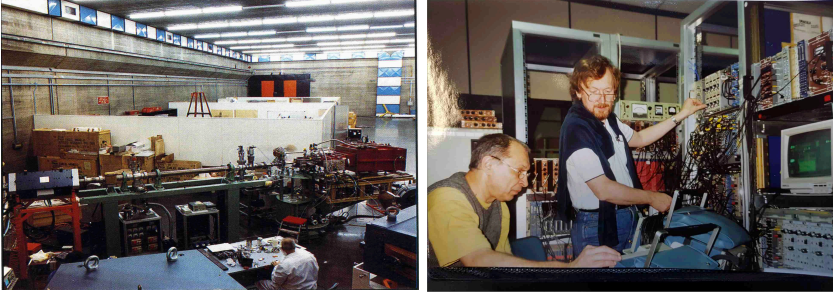
Detailed studies on dissipative phenomena in the collision of light nuclei, for several systems, were successfully done over the years. Continuous measurements of energy and angle for the detected fragments were performed. The studies concentrated on one side, on global observables correlations, interaction times extracted from experimental angular distributions, systematic features of the element distributions, cross sections, charge equilibration and comparison with microscopic dynamical models and on the other side, on excitation functions for different fragments, measured in an energy range in fine steps. The experimental results we obtained highlight the presence of dissipative processes in the interaction of light systems at incident energies below 10 MeV/nucleon. In complete analogy with medium and heavy systems, the same types of correlations between measured physical observables are established for light systems. A full dynamics from quasielastic to completely damped events is
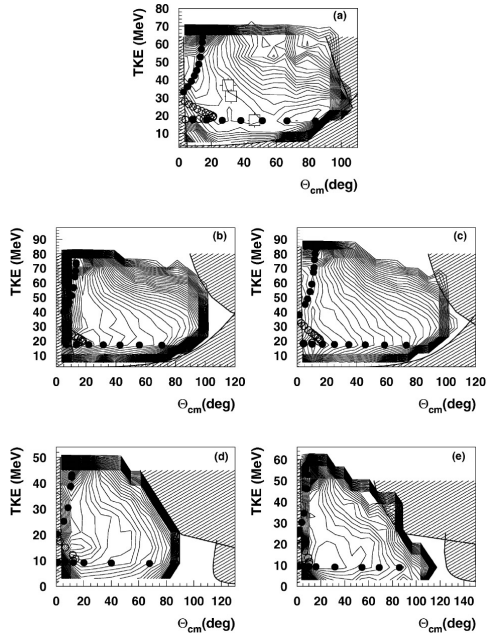
The double differential cross section $d^2\sigma/(d\theta_{cm} \, dTKE)$ as a function of the centre of mass detection angle and total kinetic energy for the ^{19}F + ^{27}Al reaction at $E_{lab} = 111.4$ MeV (a), $E_{lab} = 125$ MeV (b), $E_{lab} = 136.9$ MeV (c) and the ^{19}F + ^{12}C reaction at $E_{lab} = 111.4$ MeV (d), $E_{lab} = 136.9$ MeV (e). The hatched areas are the cuts introduced in the experimental data by the geometry and the detection threshold in energy of the experimental device. The open circles and full dots show the result of the calculations with the code DONA. Open squares in (a) are BNV calculations.

observed on an energy scale imposed by the size and incident energy of the system in interaction (see right figure).

Independently on the chosen reaction product, almost the same value of the average interaction time is obtained, as long as the corresponding angular distribut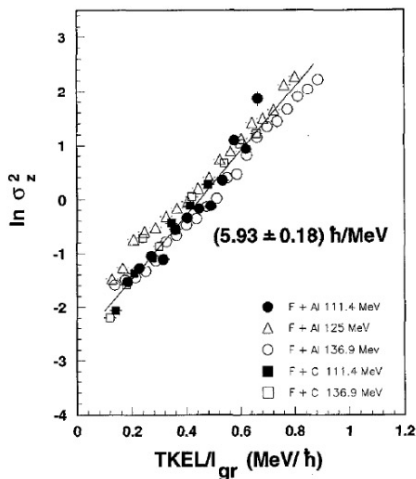ion from the same total kinetic energy loss window is analysed in order to extract it. The larger is the difference between the atomic numbers of a given reaction product and of the projectile, the larger is the corresponding energy loss and consequently the interaction time needed to reach that product. Thus, a diffusion type process is inferred. The average interaction time decreases from $\approx 10^{-21}$ s in the region of complete

Angular distributions corresponding to *TKE* windows of 6 MeV width, for the reaction products with $Z = 8$ measured in the ^{19}F (136.9 MeV) + ^{27}Al reaction. The different symbols denote the experimental data. The vertical error bars are of the order of magnitude of the symbols. The thick lines show the results of the fits with Eq. (13). The numbers on the left side are multiplicative coefficients used to represent all the data on the same figure. The *TKE* windows and the corresponding interaction time estimated as explained in the text are indicated on the right side of the figure (in parentheses is the sticking limit value).

damping up to the order of 10^{-23}s for low energy losses, being about an order of magnitude below the values characteristic to heavier nuclear systems (see left figure).

The variance of the charge distribution as a function of the total dissipated energy divided by the grazing angular momentum confirmed that the dissipative phenomena, extensively studied for medium and heavy mass colliding nuclei, also occur in light ion collisions (see figure below, left). The experimental charge distribution variance and energy dissipated per exchanged nucleon follow the same trends in the case of light, medium and heavy systems.

This is demonstrated by plotting on an universal scale the experi-

mental data multiplied by size and incident energy-dependent factors (see figure below, right).
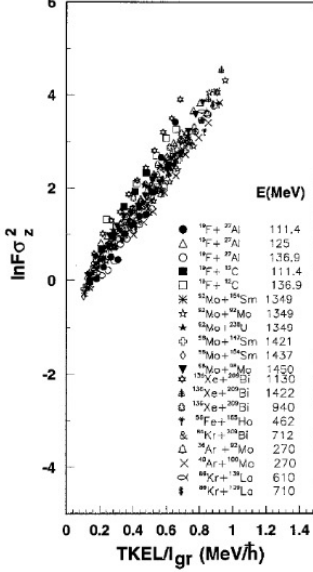
The comparison between the experimental data for the conditional charge variance and the predictions of the model for the damped quantum oscillator in the charge asymmetry degree of freedom, treated as an open quantum system, with the same parameters used for heavier systems shows good agreement. The presence in light systems of the same types of correlations as those established for medium and heavy systems, suggests the existence of similar underlying microscopic mechanisms.

Complementary to the above mentioned studies, excitation functions of the outgoing fragments in a large solid angle and energy range for two light colliding systems were measured. Large fluctuations are evidenced in all considered excitation functions. The Z and angular cross correlation analysis shows that these fluctuations are not of compound nucleus origin.

The lifetime and properties of the double nuclear system and the involved reaction mechanism are inferred from the experimental data. Steps in the analysis performed for the $^{19}F + ^{27}Al$ and $^{27}Al + ^{27}Al$ systems are exemplified below.
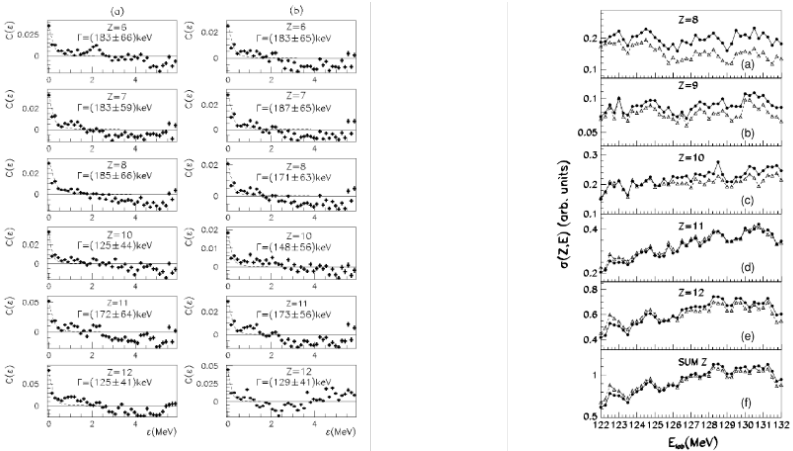
In summary, DRACULA @ LNS was a successful story and we acknowledge with

great pleasure the financial support from INFN, from the directors of LNS, sustained support from all segments of the local infrastructure and, last but not least, of the excellent crew in charge with the operation of the Tandem and Cyclotron. The friendly atmosphere felt from the first days will never be forgotten. A photo from the little party we had after a successful first experiment, in December 1991, is shown below.

The participants to the experiments were:

A.Andronic[1], I.Berceanu[1], A.Buta[1], P.Dima[1,†], M.Duma[1], I.Legrand[1], N.Mihai[1], D.Moisa[1], G. Nagel[1,†], M. Petrovici[1], A. Pop[1], V. Simion[1], A.Bonasera[2,3], G.Immé[2,3], G.Lanzanò[2,3,†], A.Pagano[2,3], G.Raciti[2,3,†], N.Colonna[4], G.d'Erasmo[4,5], A.Pantaleo[4,†], A Del Zoppo[2], R.Coniglione[2], P. Piatelli[2], P.Sapienza[2]

1. Horia Hulubei National Institute for R&D in Physics and Nuclear Engineering (IFIN-HH), Bucharest, Romania
2. Istituto Nazionale di Fisica Nucleare, Laboratorio Nazionale del Sud, Catania, Italy
3. Dipartimento di Fisica, Università di Catania, Italy
4. Istituto Nazionale di Fisica Nucleare, Sezione di Bari, Italy
5. Dipartimento di Fisica, Università di Bari, Italy
(†deceased)

For details

M. Petrovici et al., Z. Phys. A 354 (1996) 11
A. Pop et al., Phys. Lett. B 397 (1997) 25
I. Berceanu et al., Phys. Rev C 57 (1998) 2359
I. Berceanu et al., PRAMANA-journal of physics 53 (1999) 419
A. Pop et al., PRAMANA-journal of physics 53 (1999) 437
A. Pop et al., Nucl. Phys. A 679 (2001) 793
I. Berceanu et al., Phys. Rev C 74 (2006) 024601

R&D activities

Ageing studies of Multi-Strip Multi-Gap Resistive Plate Counters based on low resistivity glass electrodes in high irradiation dose

The fixed target experiment Compressed Baryonic Matter (CBM) at the future Facility for Antiproton and Ion Research (FAIR) at Darmstadt, designed to cope with interaction rates up to 10^7 events/sec for Au-Au collisions at $\sqrt{s_{NN}}=$ 2-5 GeV, will deliver the required statistics in order to perform multi-differential analysis and access rare probes, prerequisites for evidencing signatures of phase transitions or critical point of the phase diagram predicted by QCD.

The Time of Flight (ToF) sub-detector of the CBM experiment, based on multi-gap resistive plate counters, will be exposed to charged particles counting rate of $\approx 3 \cdot 10^4/\text{cm}^2$·sec and ≈ 1 hit/cm^2 at a distance of 8 meters from the target and smallest polar angles. As CBM experiment is foreseen to run 2 months/year for about 10 years, ageing tests in high irradiation dose are mandatory in order to guarantee that such a detector will maintain its performance over the whole lifetime of the experiment.

Detailed tests and analysis of ageing effects of high irradiation dose on Multi-Strip Multi-Gap Resistive Plate Counters (MSMGRPC) based on low resistivity glass electrodes, foreseen to be used for the most forward polar angles covered by ToF, were performed at a multi-purpose irradiation facility of IFIN-HH using a ^{60}Co source. The MSMGRPC dark curent and dark counting rate, efficiency, cluster size, surface and volume resistivity of the glass electrodes after irradiation were measured and compared with their values before irradiation. In two weeks after irradiation their values were the same as the ones before irradiation. Nevertheless, visible layers deposited on both sides of the glass electrodes and ablation type patterns were observed after disassembling the irradiated MSMGRPC.
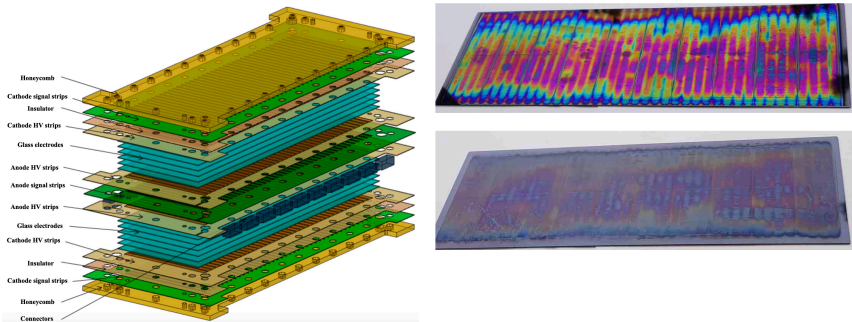
A comprehensive analysis of the composition and properties of the deposited layers

on the glass electrodes, based on different methods, i.e. Scanning Electron Microscope (SEM), X-ray Photoelectron Spectroscopy (XPS), foil Elastic Recoil Detection Analysis (ERDA), Rutherford Backscattering Spectrometry (RBS), Atomic Force Microscopy (AFM), Terahertz Time Domain Spectroscopy (THz-TDS) and Energy Dispersive X-ray analysis (EDX) were performed. A schematic architecture of a double sided MSMGRPC is presented in the figure above, on the left.

The MSMGRPC was operated for about 40 hours in a total cumulated dose of 13 kGy. In the figure above, on the right the photos of the two sides of a floating resistive glass electrode: the surface facing the cathode electrode (top) and the surface facing the anode electrode are presented (bottom).

Some of the results of EDX investigations on the elemental composition of some samples of surfaces are presented below, for the anode and cathode surfaces of a glass electrode after irradiation of MSMGRPC. The fluorine percentage on the surface of glass electrodes used in the MSMGRPC operated in high irradiation dose is significant and different for the two surfaces. The anode surface contains 31.73±0.3% fluorine relative 18.81±0.2% found on the cathode surface. As far as concerns the oxygen, relative to 46.10±0.3% corresponding to non irradiated glass plate, the values obtained for the irradiated glass plate are 23.12±0.2% and 36.42±0.3% for the two surfaces, respectively.

Full scale counts: 56866
Integral Counts: 2322611 — Extracted Spectrum

Element	Extracted Spectrum				
	Net Counts	Weight%	Weight% err	Atom %	Atom % err
O K	218509	15.88	0.07	23.12	0.19
F K	280231	25.87	0.10	31.73	0.25
Na K	270828	20.02	0.08	20.29	0.16
Al K	91370	3.59	0.03	3.10	0.05
Si K	499986	17.42	0.05	14.45	0.08
S K	3974	0.14	0.01	0.10	0.01
Cl K	5725	0.21	0.02	0.14	0.02
K K	1878	0.07	0.01	0.04	0.01
Ca K	1290	0.05	0.01	0.03	0.01
Fe K	192129	16.74	0.07	6.99	0.06
		100.00		100.00	

Full scale counts: 73218
Integral Counts: 2463542 — Extracted Spectrum

Element	Extracted Spectrum				
	Net Counts	Weight%	Weight% err	Atom %	Atom % err
O K	329097	24.64	0.09	36.42	0.25
F K	127222	15.11	0.08	18.81	0.20
Na K	197859	15.15	0.07	15.59	0.14
Al K	126132	4.77	0.03	4.18	0.05
Si K	539958	18.44	0.05	15.52	0.09
P K	1447	0.06	0.01	0.05	0.02
S K	4388	0.16	0.02	0.12	0.02
Cl K	7014	0.26	0.01	0.17	0.01
K K	7869	0.29	0.01	0.18	0.01
Ca K	3411	0.14	0.02	0.08	0.02
Fe K	245991	20.99	0.08	8.89	0.07
		100.00		100.00	

Left-top: electron spectra corresponding to anode surface of irradiated glass; Left-bottom: the corresponding relative elemental composition. Right-top: electron spectra corresponding to cathode surface of irradiated glass; Right-bottom: the corresponding relative elemental composition.

These findings were confirmed by the other types of analyses mentioned above. The surfaces scanning using AFM, evidenced larger peak to valley structures on the surfaces of irradiated glass electrodes relative to the non-irradiated ones. The THz-TDS analysis evidenced negligible changes in the dielectric constants of irradiated floating electrodes, the estimated impact on the transmission line impedance being

of the order of a few percent. Therefore, no major impact on the impedance matching to the one of the frontend electronics is expected. The measured surface and volume resistivity of the floating glass electrodes and of the glass electrodes in direct contact with the high voltage electrodes of the irradiated MSMGRPC were found to be the same as for the non-irradiated glass plates.

These studies were performed using a housing box flashed with the working gas mixture. Therefore, the gas exchange in the 140 μm 10 gas gaps of the counter is via a diffusion process. It is well known that the polymerisation phenomenon is inversely proportional with the gas flow. A directed gas flow through the gas gaps is expected to decrease the observed ageing effects. Such a new architecture is in progress to be realised. Based on the produced charge in the counter during the operation in the high irradiation dose and the charge produced by a minimum ionising particle, we estimated more than $3 \cdot 10^5$ avalanches/cm^2·sec, 10 times higher than the counting rate expected at CBM for the most forward region, i.e. low polar angles. Besides an increase of the gas flow through the gas gaps, an exposure to a lower dose and longer time, conclusive for the operating conditions in the CBM experiment, will be performed.

For details

D. Bartoş et al., Nucl. Instrum. Meth. A 1024 (2022) 166122

# TRD-2D DAQ integration into mCBM

During the first months of 2021 the development of a local DAQ chain for TRD-2D, prepared for integration in mCBM DAQ (still in development at that time) was finished. The resulting DAQ was used to test the detector and frontend electronics for integration in mCBM. Various firmware modules were later used in the development of the TRD-2D-specific firmware for CRI1 (Common Readout Interface).
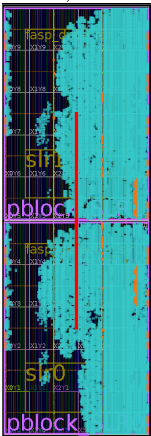

After completing the local tests, the detector and the frontend electronics were transported at GSI and installed in mCBM. In parallel, the CRI1 firmware for TRD2D was developed. The development used the CBM workflow and all the required common components, resulting in a full integration of TRD-2D into CBM DAQ. With the integrated DAQ, TRD-2D participated in mCBM campaign of July 2021 when synchronous operation (TFC mode) of several subdetectors was achieved. After the mCBM July campaign the development continued by identifying and fixing some bugs, in particular a mapping bug introduced when switching from the local DAQ chain firmware to CRI1 firmware. A qualitative representation of the FPGA areas used by the firmware develop for the CBM compatible DAQ is presented in the figure on the left. We also participated in the mCBM December campaign, both for dry-run and cosmics-run.

RPC @ mCBM

T wo MSMGRPC prototypes with a 200 μm gas gap were assembled and successfully tested with cosmic rays in HPD/IFIN-HH, showing a very good efficiency and time resolution. These prototypes were tested in-beam in the mCBM experimental setup installed at SIS18 acceleration facility of GSI Darmstadt. At low counting rate an efficiency plateau around 96% and a single counter time resolution of the order of 40 ps were obtained. A scan with the beam intensity was converted in the incident particle flux on the chamber. At the highest intensity, a landmark value for the inner zone of about 25 kHz/cm^2 particle counting rate was reached, with exposure on the whole active area of the counter.

The nicely reproduced beam spill shape show the counter performance at the highest counting rate (see figure below).
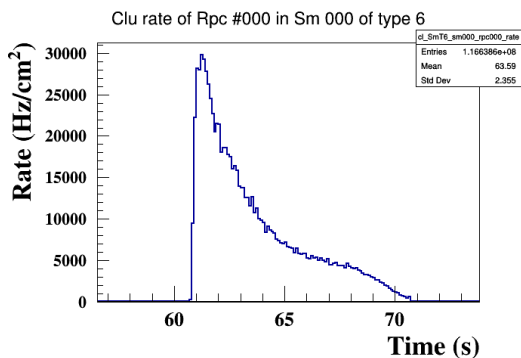
The measured efficiency (bottom left figure) and time resolution (bottom right figure) are still very good, deterioration with the counting rate being minor.
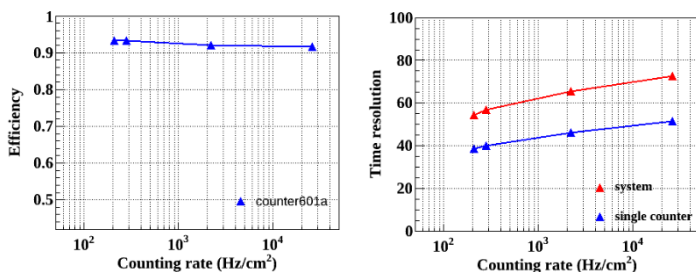
For the mitigation of the ageing effects, we proposed a new detector architecture with a directed gas flow through the gas gaps. The new prototype was assembled, preliminary tested in the DetLab of HPD and in-beam in July 2021 within the mCBM setup.
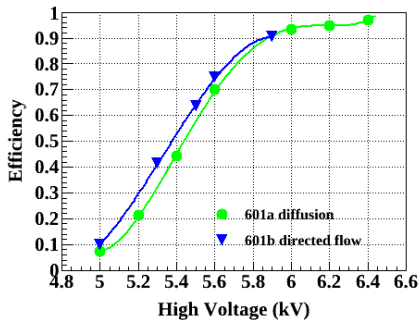
The obtained results, in terms of efficiency (blue symbols) are similar with the results obtained for the previous prototype (green symbols), with gas exchange via diffusion (see the figure above). A similar behaviour as a function of high voltage is observed. A single counter time resolution of 52 ps was obtained.

For details

M. Petriş et al., CBM Technical Note (2021), CBM-TN-21004
D. Bartoş et al., Nuclear Inst. and Meth. in Phys. Res. A 1024 (2022) 166122
M. Petriş et al., 38th CBM Collaboration Meeting, 27.09. - 1.10, 2021

TRD-2D joined the mCBM setup

The CBM Collaboration has organised a dedicated target area at GSI, since 2018, for high beam intensity experiments where a test stand for electronics and detector integration, denoted as mCBM is located. Using the SIS18 accelerator a variety of target-projectile configurations and interaction rates were thus accessible. The physics target of the mCBM experiment is the reconstruction of lambda by its decay in the pion and proton channel.

Participating in the mCBM experiment for the first time in July 2021, the TRD-2D prototype, the FASP based Front End Electronics (FEE) and CBM compatible data processing, all developed in our department during the last 15 years, were fully integrated with the rest of the CBM components. An annotated picture taken during the mechanical installation of the TRD-2D modules in the experimental cave is displayed in the following figure together with the simulated geometry. The TRD-2D technology was represented at mCBM by two modules; a close to final version (TRD-2D in the figure) and a reduced size one, having read-out connections for both the FASP and SPADIC FEEs, identified as TRD-2Dh in the figure.

Both TRD-2D detectors were operated using the common DAQ framework based on GBTx serializer and CRI boards concentrators developed for CBM. Alongside
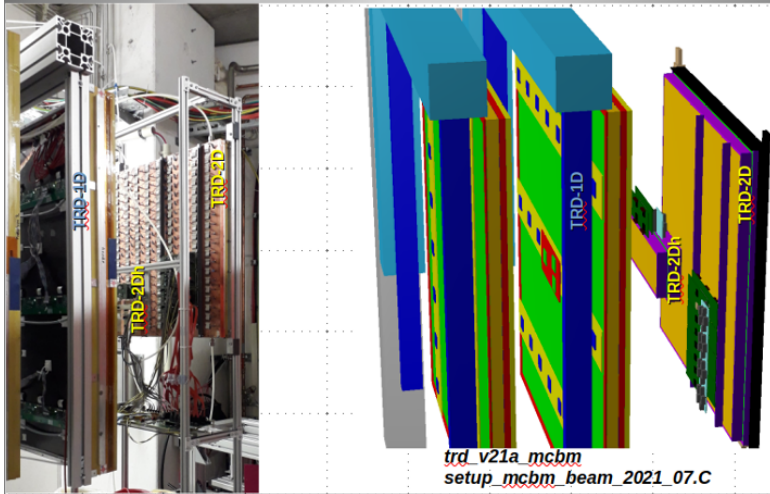
The relative positioning of the TRD-2D prototypes within the mCBM experiment; a picture from the experimental cave (left) and the geometrical setup as used in simulations (right).

TRD-2D other future CBM components like STS, TRD-1D, ToF, RICH and PSD were operated. The data from all six systems provides for the first time a correlated view of the future CBM data structure and also the possibility to improve the matching between such independent components. In the bottom figure, a view of the data flux for each system is presented. It emphasises the spill of the structure, the ratio of S/N for each system during beam on intervals, and the response of the system following the increased rate of the spill towards its end. The TRD-2D(FASP) data taking shows one of the best S/N ratio following the spill structure. A preliminary test of endurance to high data rates was also performed successfully for the FASP electronics.
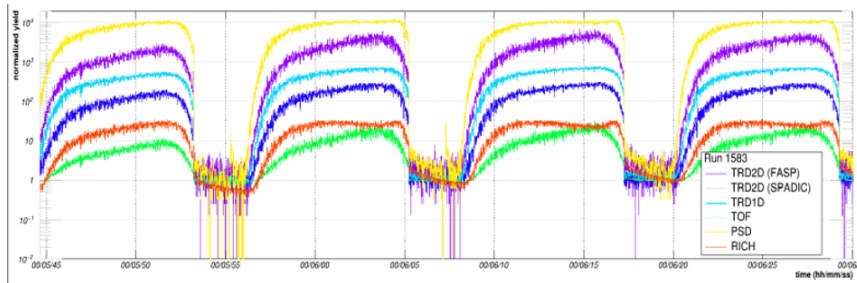
The data flux from each mCBM component of the 2021 data taking campaign.

A second step of detector integration was to construct "raw events" by registering the system data which are timely correlated with a reference system.

In the figure on the right, such correlation is presented using ToF as reference. The excess of data which appears around dt = 0 are data correlated with the reference while the white background suggests uncorrelated data. The quality of the time correlation is further emphasised by the Gauss fit to the data. Values of the binary system time resolutions are also added for quantification.
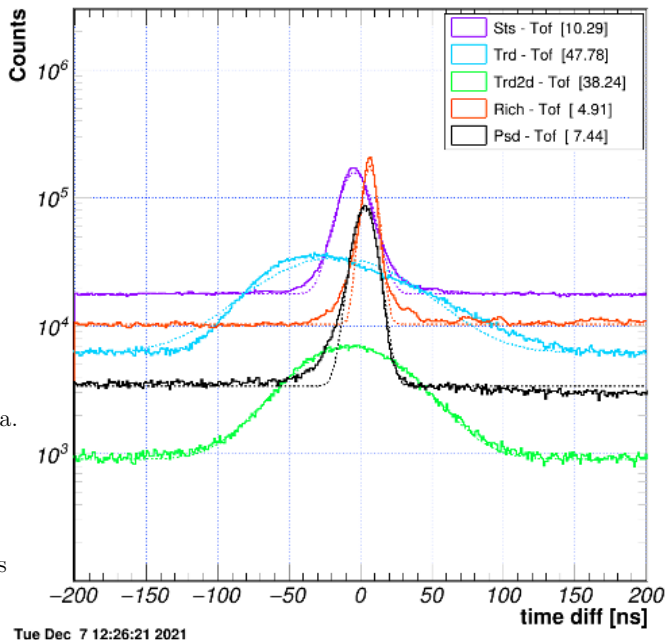

Time correlation between the data of each mCBM components and a reference selected here to be the ToF system.

The TRD-2D is very accurately described by the statistical model with a time resolution in accordance with the theoretical understanding of the system. A final test of system integration in the mCBM was performed by following linear trajectories of particles being detected by several systems. Three mCBM systems have similar position information capabilities available at data processing level, the STS, TRD-2D and ToF.

Based on the time-correlation analysis, the data candidates generated by the same interaction ("raw event") are reconstructed. Linear correlations wrt. the ideal vertex at position (0,0,0) are used to estimate spatial resolutions. In the following figure, such spatial correlations between reconstructed hits in TRD-2D and linear projections from vertex of ToF and Sts hits are displayed on the horizontal (dx) and vertical (dy) directions. This very first results suffer heavily from mis-alignment and vertex definition but they show, for the first time, a clear spatial correlation of the three detectors and a background of uncorrelated hits. Although very poor, the "event" integrated spatial resolution of approx. 7 cm is still a factor 2 better than what can be obtained if only STS and ToF are used.

A golden milestone was reached in our TRD-2D R&D project by demonstrating the full integration of the TRD-2D system with the CBM infrastructure. The first performances reported here, although far from the target, are demonstrating the
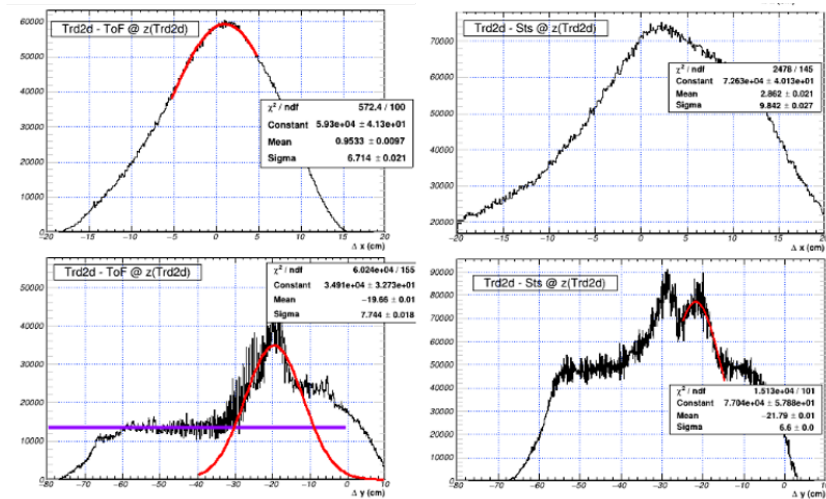
Spatial resolution in the horizontal (dx) direction (upper row) and vertical (dy) direction (bottom row) between TRD-2D wrt. the ToF (left) and STS (right) detectors, respectively.

soundness of our proposal and open large perspectives for the future of this system within the CBM collaboration.
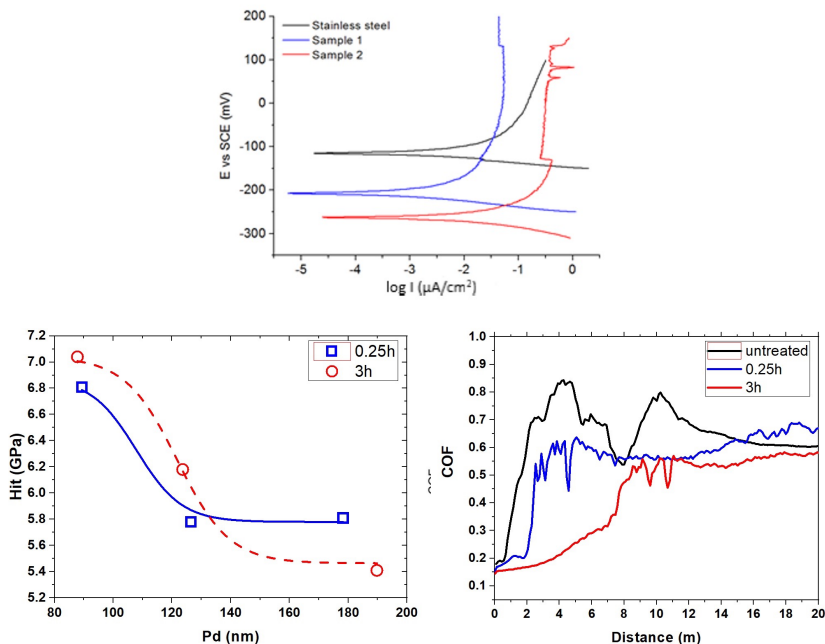
For details

https://m.facebook.com/watch/?v=1319090865232740&_rdr.

Applied Research

Improvement of mechanical, corrosion and wear resistance properties of stainless steel by surface nitriding in open atmosphere cold plasma

O pen atmosphere cold plasma nitriding represents a low-cost alternative to the vacuum plasma ion nitriding process for the improvement of mechanical, corrosion and wear resistance properties of stainless steel, especially for large dimension industrial tools. Two samples of stainless steel were treated in open atmosphere cold plasma using only nitrogen as working gas, first sample for 0.25 hours and the second one for three hours. The treated stainless steel surfaces had a granular homogenous morphology and presented an increase of surface roughness led probably by the formation of more compact and higher aggregates. The corro-

sion resistance has improved for the nitrided samples decreasing the potential and increasing the treatment time. An increased hardness was observed for the treated surfaces and the highest hardness values were measured at the lowest penetration depth. A low friction regime was noticed for the nitrided samples for a relatively short sliding length that increased with longer treatment process (see the figure below).
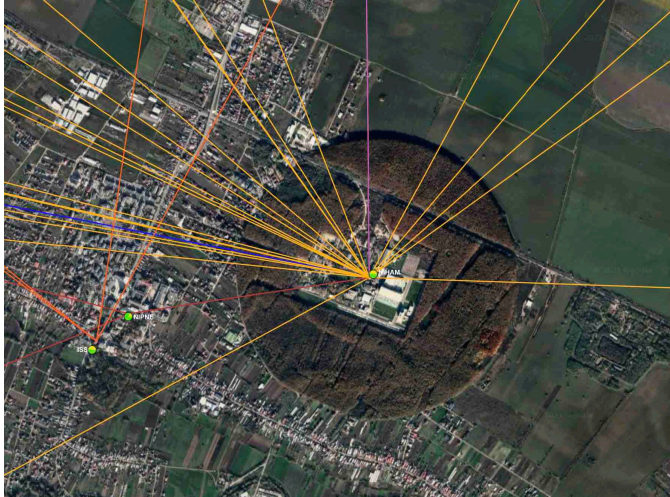

For details

A. O. Mateescu, G. Mateescu, A. Balan, C. Ceaus, I. Stamatin, D. Cristea, C. Samoila and D. Ursutiu, Materials, 14 (2021) 4836

Infrastructure

Computing

T he HPD Data Centre NIHAM is a Tier2 component of the ALICE GRID. NIHAM maintains its efficiency within the ALICE GRID.

Last year $4.2 \cdot 10^6$ jobs were processed within 6.9 Mhours computing time, which amounts to 4.6% and 2.45% of Tier2 contributions to ALICE GRID, respectively. A snapshot of the connections between NIHAM and the other GRID centers of ALICE is presented on the figure above.

For details

```
http://alimonitor.cern.ch/map.jsp
```

Open Atmosphere Cold Plasma Surface Treatment

A new Laboratory for cold plasma surface treatment in open atmosphere has been set up and equipped with the corresponding instrumentation.
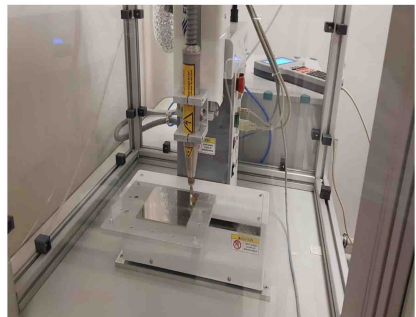
First tracks recorded with the upgraded ALICE-TPC

After almost 3 years of LS2, on October 27th 2021, a first stable beam in LHC, injected from SPS, was obtained. The very first tracks recorded with the upgraded ALICE-TPC can be seen in the figure below.
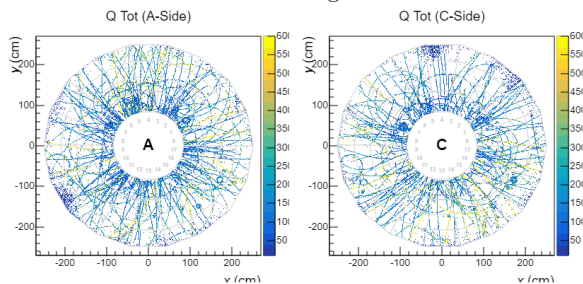
It is worth mentioning that 50% of the Outer Read Out Chambers (OROCs) of ALICE-TPC, based on GEM technology, delivering the information on which such reconstructed tracks are obtained, were assembled and tested in the Hadron Physics Department.

Summer Student Program

We will organise the HPD Summer Student Program, the successful previous editions being interrupted in 2020 and 2021 by the pandemic circumstances. If the situation remains the same we could host in person only three students, for each of them being able to offer separate offices. If the evolution of the COVID-19 pandemic will allow, the number of the selected students will increase, being limited by the selection criteria based on the requested information in the application (`http://niham.nipne.ro/2022_SSP_details.pdf`).

For details

`http://niham.nipne.ro/program_studenti.html`

Students' Activity

Theses

PhD thesis

M. G. Târzilă	Study of collective type phenomena in p+p collisions at the highest energy accessible at LHC using the ALICE experimental set-up

Bachelor thesis

D. I. Dorobanțu	Studies of ageing of Multi-Strip Multi-Gap Resistive Plates Counters in high irradiation dose

International events

Talks

A. S. Mare	From Nuclear Structure and Dynamics to rp-Process Nucleosynthesis in X-Ray Bursts
	Carpathian Summer School of Physics, 18-27 August 2021, Sinaia, Romania
A. Lindner	Geometrical scaling for light flavor hadrons
	Particles and Nuclei International Conference, 5–10 September 2021, Online

Poster

A. Lindner	Geometrical scaling for strange and multi-strange hadrons in pp and A-A collisions at relativistic energies
	European Physical Society conference on High Energy Physics, 26-30 July 2021, Online

Schools

A. Lindner A. S. Mare	Carpathian Summer School of Physics, 18-27 August 2021, Sinaia, Romania
A. Lindner	CERN-Fermilab Hadron Collider Physics Summer School, 23 August - 4 September 2021, Online

Visits

Obviously, due to the present pandemic situation, the number of in person visits to Hadron Physics Department was reduced relative to the previous years. However, following the protection rules, we hosted quite a few successful ones.

It is worth mentioning the visit of a group of German students (see photo on the left), the participants being impressed by the R&D activities, the results, the infrastructure, the lively atmosphere.

We were honoured to be visited by the Charge d'Affaires of American Embassy in Romania, being impressed by his interest to go in some details of our activities and results.

Recently, our Department was visited by the Minister of Research, Innovation and Digitalization, Marcel Ioan Bolos and the State Secretaries Iulian Vasile Popescu and Tudor Prisecaru.

Celebrating the 125th year of the birth of Horia Hulubei

The present issue of the Hadron Physics Courier is dedicated to Horia Hulubei, the founder of the Physics Institute of the Romanian Academy, followed by the Institute of Atomic Physics, the precursor of the present Institutes on Magurele site, the main one being the Institute for Physics and Nuclear Engineering (IFIN-HH).

Job opportunities

Physicist

Physicist from master student to postdoc level, to be involved in Experimental Heavy Ion Nuclear Physics. The successful candidate will participate in research with members of the Hadron Physics Department from IFIN-HH, focusing on the new generation of detectors construction, simulations, tests and their implementation in the CBM Experiment at FAIR. The candidate will also be involved in data analysis obtained in the test experiment at mCBM or in ALICE Experiment during Run3, starting from 2022.

Electronic Engineer

PhD or postdoc with some experience in CHIP design to be involved in development of analog and digital CHIPs for dedicated front-end electronics for the detectors developed in Hadron Physics Department for the present and future experimental devices. The successful candidate will also participate in the test activities of the present CHIPs designed in HPD and the associated mother boards. The candidate should have knowledge on FPGA programming. The activities will be related to the CBM Experiment at FAIR and later to the future Heavy Ion Experiment at LHC.

Technician

Technician with a post high school certificate. The successful candidate will be involved in preparation of detector components, detector construction, operation and tests, maintenance and operation of the DetLabs infrastructure.
Selected candidates will have a temporary position for 1 year with the possibility to be extended to 2 years. In case of high performance and adequate involvement in the HPD activities, the position could become permanent.

Contact
Prof. Dr. Mihai Petrovici
Email: mpetro@nipne.ro

Editors
Amelia Lindner, Adrian Sorin Mare, Mihai Petrovici
Production editor: Adrian Socolov

Electronic version
HPD Couriers can be accessed at: http://niham.nipne.ro/HPD_Courier.html

Horia Hulubei

(1896-1972)

Founder of the Atomic Physics Institute